

Giant magnetoresistance behavior of an iron/carbonized polyurethane nanocomposite

Zhanhu Guo,^{a)} Sung Park, and H. Thomas Hahn

Mechanical and Aerospace Engineering Department, University of California, Los Angeles, Los Angeles, California 90095 and Materials Science and Engineering Department, University of California, Los Angeles, Los Angeles, California 90095

Suying Wei

Department of Chemistry, Louisiana State University, Baton Rouge, Louisiana 70803

Monica Moldovan, Amar B. Karki, and David P. Young

Department of Physics and Astronomy, Louisiana State University, Baton Rouge, Louisiana 70803

(Received 2 November 2006; accepted 21 December 2006; published online 1 February 2007)

This letter describes the magnetoresistance (MR) behavior of the heat treated polyurethane composites reinforced with iron nanoparticles. The flexible nanocomposites were fabricated by the surface-initiated-polymerization method. The uniformly distributed nanoparticles within the polymer matrix, well characterized by field emission scanning electron microscopy, favor a continuous carbon matrix formation, rendering the transition from insulating to conductive composites. The coercive forces reflect strong particle loading and matrix dependent magnetic properties. By simply annealing in a reducing environment, the obtained nanocomposites possess a MR of 7.3% at room temperature and 14% at 130 K occurring at a field of 90 kOe. © 2007 American Institute of Physics. [DOI: 10.1063/1.2435897]

Polymer nanocomposites with functional particles have spurred much interest due to their cost-effective processability and high flexibility, rendering possible many applications such as microwave absorbers,¹⁻³ photovoltaic (solar) cells,⁴ and smart structure.^{5,6} Incorporation of inorganic nanofillers into a polymer matrix can stiffen and strengthen the nanocomposites,⁷ increase the electric and thermal conductivities,^{8,9} and even improve the shape replicability.¹⁰ Since the discovery of multilayer giant magnetoresistance (GMR) effect in 1988,¹¹ GMR has found wide applications in areas such as biological detection,¹² magnetic recording and storage systems,¹³ and rotational sensors in automotive systems.¹⁴ Compared with metallic GMR sensors, the polymer nanocomposite GMR sensors would have the benefit of easy and cost-effective fabrication. However, the problem is with the difficulty of obtaining a high volume fraction of nanoparticles uniformly dispersed throughout the polymer matrix.

In this letter, we report on the processing and characterization of a granular GMR nanocomposite that consists of iron particles dispersed in a carbon matrix. The processing starts with the fabrication of a polyurethane matrix composite reinforced with nanoparticles (NPs) having an iron core/iron oxide shell structure and an approximate diameter of 20 nm (provided by QuantumSphere Inc.). The surface-initiated-polymerization (SIP) method¹⁵⁻¹⁷ allows a high loading, up to 65 wt %, of NPs to be incorporated into the polymer. In the SIP method, both the catalyst (a liquid containing aliphatic amine, parachlorobenzotrifluoride, and methyl propyl ketone) and the accelerator (polyurethane STD-102, containing organotitanate) are added into an iron-nanoparticle suspended tetrahydrofuran solution. The two-part monomers (diisocyanate and diol, CAAPCOAT FP-002-55X, CAAP Co., Inc.) are introduced into the above solution

to polymerize for 6 h, and then poured into a mold for curing. All the operations are carried out with ultrasonication.

Nanocomposites with two different particle loadings of 35 and 65 wt % were fabricated by the SIP method. They were heat treated at 250 °C for 2 h in hydrogen gas balanced with ultrahigh purity argon (5%). In order to carbonize the matrix, the nanocomposite with 65 wt % particle loading was further heat treated at 450 °C for 2 h in the same environment. Particle structures were characterized on a JEOL transmission electron microscope (TEM) (JEOL TEM-2010). The valence state in the Fe NPs was determined by x-ray photoelectron spectroscopy (XPS). Weight percentage of NPs in the nanocomposites was determined by the thermogravimetric analysis (PerkinElmer) with an argon flow rate of 50 cm³/min. The polyurethane, particle loading, and heat treatment effect on the magnetic properties were investigated in a 9 T physical properties measurement system by Quantum Design. The electric conductivity and magnetic field dependent resistance were carried out using a standard four-probe method.

Figure 1 shows the TEM bright field microstructures of the as-received NPs. The obvious contrast within the particle in Fig. 1(a) is due to the oxidation of the Fe nanoparticle surface. XPS studies show that the iron oxide is Fe₂O₃ rather than other oxides (FeO and Fe₃O₄). The lattice distances of 0.204 nm (ring 1), 0.143 nm (ring 3), 0.116 nm (ring 4), 0.100 nm (ring 5), and 0.083 nm (ring 6) of the selected area electron diffraction (SAED) in the inset of Fig. 1(a) can be assigned to (110), (200), (211), (220), and (222) planes of Fe;¹⁸ and 0.167 nm (ring 2) arises from the (430) plane of Fe₂O₃.¹⁹ The clear lattice fringes shown in Fig. 1(b) indicate a high crystallinity of the NPs. The discontinuous fringes indicate the existence of a small number of defects within the NPs. The calculated fringe spacing of 0.350 nm corresponds to the standard (211) plane of Fe₂O₃ with a reported *d* spac-

^{a)}Electronic mail: zhanhu@seas.ucla.edu

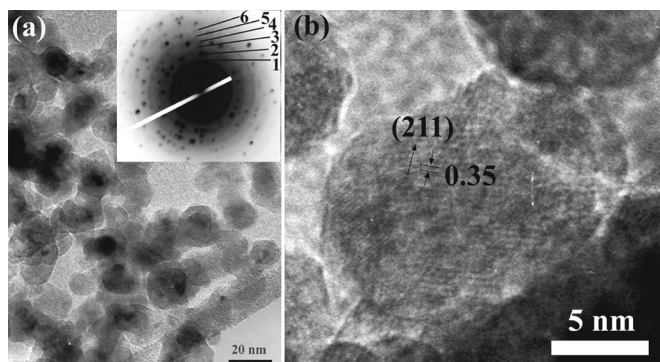


FIG. 1. (a) TEM and (b) high-resolution transmission electron microscopy (HRTEM) micrographs of as-received NPs. The inset shows SAED.

ing of 0.3411 nm,¹⁹ partial oxidation of the Fe NPs, consistent with SAED analysis.

Figure 2 shows the TEM bright field microstructures of the nanocomposite (65 wt %) after heat treatments at 250 °C for 2 h and 450 °C for additional 2 h. There is almost no microstructural change in the first heat treatment stage (250 °C), and the nanocomposite has little mass loss. However, a large shrinkage is observed in the second stage (450 °C), indicating decomposition of the polymer. The inner ring of the SAED patterns with a d spacing of 0.34 nm in the inset of Fig. 2(a) clearly indicates the formation of graphite carbon. Clear lattice fringes shown in Fig. 2(b) of high-resolution TEM indicate the formation of highly crystalline NPs. The calculated lattice distance of 0.21 nm corresponds to Fe NPs, and the surrounding lattice fringe spacing of 0.34 nm corresponds to the (002) plane of graphite carbon. This indicates that Fe NPs are embedded in a carbon matrix. No oxides observed remaining in the NPs indicate that the high-temperature heat treatment favors the reduction of iron oxides.

The particle distribution within the polyurethane matrix before the heat treatment was characterized by a scanning electron microscope (SEM). The samples were prepared by embedding the flexible composite in a cured vinyl-ester tab and polishing with 4000 grit sandpaper. The inset of Fig. 3 shows typical SEM images of the cross-sectional area of the nanocomposite with a particle loading of 65 wt %. The uniform particle distribution and no obvious particle agglomeration indicate that the SIP method yields a high-quality nanocomposite, as compared with a direct mixing method which results in a brittle nanocomposite.

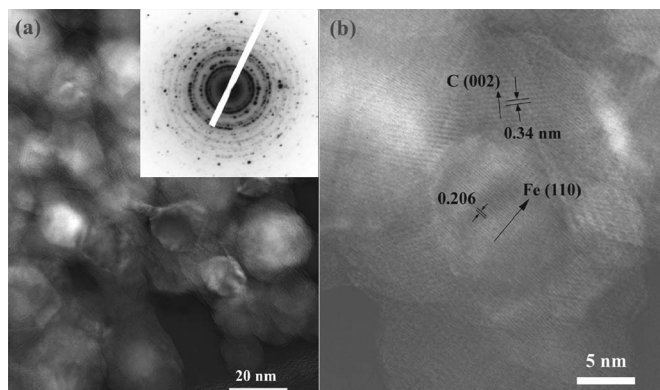


FIG. 2. (a) TEM and (b) HRTEM micrographs of the nanocomposite with a 65 wt % loading after heat treatment at 450 °C. The inset shows SAED.

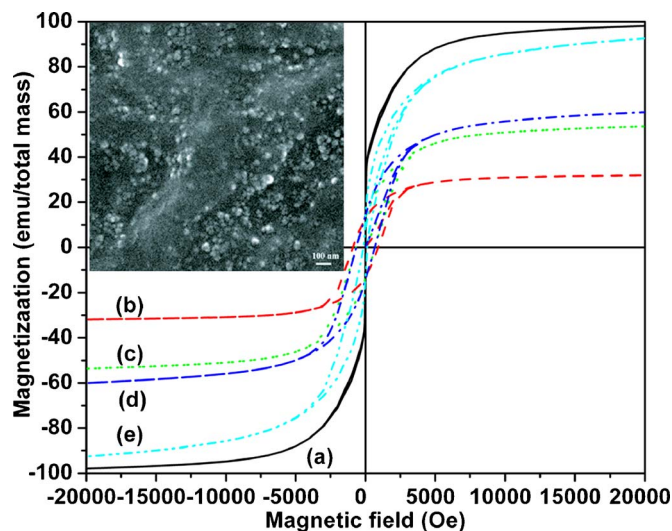


FIG. 3. (Color online) Hysteresis loops of (a) as-received NPs; nanocomposites with a particle loading of (b) 35 wt % and (c) 65 wt %; and nanocomposite with 65 wt % particle loading with heat treatment at (d) 250 °C for 2 h and (e) 450 °C for additional 2 h. The inset shows the SEM image of nanocomposite with a 65 wt % particle loading.

Figure 3 shows the room-temperature hysteresis loops of the as-received NPs and the nanocomposites. The saturation magnetization (M_s , 97.6 emu/g, based on the total mass) of the as-received NPs is lower than that of the pure bulk Fe (218 emu/g),²⁰ which is as expected because of the presence of oxide shells. The lower coercive force (coercivity H_c : 5 Oe) indicates superparamagnetic behavior of the as-received NPs. Little difference in M_s is observed for the NPs after they are embedded in the polymer matrix. The saturation magnetizations of the nanocomposites, 54 and 31.6 emu/g for the particle loadings of 65 and 35 wt %, respectively, correspond to 84 and 90.2 emu/g for the nanoparticles. The slightly lower M_s in the nanocomposites than in the as-received NPs may be attributed to the further oxidation of the NPs during the nanocomposite fabrication process and the particle-polymer surface interaction effect.²¹ The coercivities of the polyurethane nanocomposites are 685 and 900 Oe for 65 and 35 wt % loadings, respectively, which are much larger than that of the as-received NP assembly. Such behavior, however, is typical of magnetic nanocomposites as explained later.

The heat treatment at 250 °C does not show any significant changes in mass, volume, M_s , or H_c , indicating good thermal stability of the nanocomposite. However, the heat treatment at 450 °C brings about many changes. First of all, it carbonizes the matrix and reduces the oxide shells. The mass loss and shrinkage in the matrix effectively increase the particle loading for the composite. All these changes effectively increase M_s while reducing H_c .

In the 65 wt % nanocomposite, H_c remains practically the same after heat treatment at 250 °C but decreases to 165 Oe after the additional heat treatment at 450 °C. This trend is due to the interparticle dipolar interaction within the nanocomposite with a good dispersion of single-domain NPs, consistent with particle-loading-dependent coercivity in nanoparticle assembly.²² Compared with the 35 wt % nanocomposite, the smaller coercivity in the 65 wt % nanocomposite arises from the decreased interparticle distance concomitant with a stronger dipolar interaction. The further

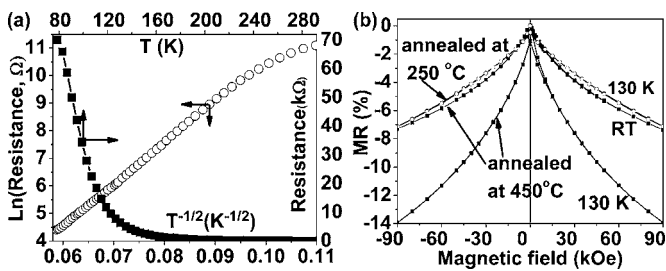


FIG. 4. Nanocomposite with a 65 wt % particle loading: (a) resistance as a function of temperature after heat treatment at 450°C , and (b) MR vs applied field at room temperature and 130 K.

decrease in H_c after the 450°C heat treatment is for the same reason, i.e., the decreased interparticle distance resulting from shrinkage. In addition, the presence of an oxide shell around the metallic core is reported to increase the blocking temperature of NPs through the exchange coupling interaction between the ferromagnetic metal core and the antiferromagnetic oxide shell.²³ Thus, the loss of the exchange coupling in the heat treated nanocomposites due to the disappearance of antiferromagnetic oxide shell also contributes to the smaller coercivity.

No electrical conductivity is detected in the polyurethane nanocomposites, even at 65 wt % loading, indicating that the particle loading is still lower than the percolation threshold. The conductivity improves considerably after the heat treatment. Figure 4(a) shows the temperature dependent resistance of the 65 wt % nanocomposite after heat treatment at 450°C . The resistance increases dramatically with decreasing temperature, characteristic of a nonmetallic behavior. Equipment limitations precluded us from measuring the resistance at temperatures below 80 K. Contrary to the as-prepared nanocomposites, those heat treated at 250°C show somewhat improved electric conductivity. However, the resistance is still about ten times higher than that of the 450°C heat treated specimen. Also, the lowest possible measurement temperature decreases from 125 to 80 K as the heating temperature is increased from 250 to 450°C . In view of the high conductivity of iron, the high resistance observed in the 450°C heat treated specimen is due to the poor conductivity of the carbon matrix. The observed linear relationship between the logarithmic resistance and the square root of temperature $T^{-1/2}$ shown in Fig. 4(a) indicates an interparticle tunneling/hopping conduction mechanism.²⁴

Figure 4(b) shows the MR as a function of the applied magnetic field H , where MR (%) is defined as: $\text{MR}(\%) = (R(H) - R(0))/R(0) \times 100$. The 250°C heat treated nanocomposite has a MR of 7% at 130 K, whereas the 450°C heat treated nanocomposite shows a MR of 7.3% at room temperature and 14% at 130 K, all at a fairly high field of 90 kOe. Compared with multilayered GMR materials, a high magnetic field is required to saturate the MR, which is a characteristic of the tunneling conduction mechanism. However, a 2% MR observed at 4 kOe still indicates that this GMR sensor could be used for biological targeting application.²⁵ An initial adsorption test shows that the heat treated nanocomposite has a fairly high porosity adsorbing about 7 wt % of argon; indicating that this composite can be

used for water distillation,²⁶ as well as for tail gas catalysis or hydrogen storage²⁷ for fuel cell applications.

In conclusion, we have shown that a granular GMR nanocomposite can be synthesized using the SIP to accommodate a high particle loading required and the subsequent heat treatment to induce carbonization of the matrix and reduce oxide shells in the NPs. The final iron/carbon nanocomposites exhibit a room-temperature GMR of 7% at 90 kOe, indicating a spin-dependent tunneling/hopping conduction.

This work was partially supported by the Air Force Office of Scientific Research through AFOSR Grant No. FA9550-05-1-0138 with B. Les Lee as the Program Manager. One of the authors (D.P.Y.) kindly acknowledges support from the National Science Foundation under Grant No. DMR 04-49022. Partial financial support from QuantumSphere Inc. is kindly acknowledged.

- ¹B. Sareni, L. Krahenbuhl, A. Beroual, and C. Brosseau, *J. Appl. Phys.* **80**, 4560 (1996).
- ²C. Brosseau, P. Queffelec, and P. Talbot, *J. Appl. Phys.* **89**, 4532 (2001).
- ³J. Liu, M. Itoh, and K.-I. Machida, *Appl. Phys. Lett.* **88**, 062503 (2006).
- ⁴W. J. E. Beek, M. M. Wienk, and R. A. J. Jassen, *Adv. Mater. (Weinheim, Ger.)* **16**, 1009 (2004).
- ⁵H. Koerner, G. Price, N. A. Pearce, M. Alexander, and R. A. Vaia, *Nat. Mater.* **3**, 115 (2004).
- ⁶R. Mohr, K. Kratz, T. Weigel, M. Lucka-Gabor, M. Moneke, and A. Lendlein, *Proc. Natl. Acad. Sci. U.S.A.* **103**, 3540 (2006).
- ⁷Z. Guo, T. Pereira, O. Choi, Y. Wang, and H. T. Hahn, *J. Mater. Chem.* **16**, 2800 (2006).
- ⁸S. Stankovich, D. A. Dikin, G. H. B. Dommett, K. M. Kohlhaas, E. J. Zimney, E. A. Stach, R. D. Piner, S. T. Nguyen, and R. S. Ruoff, *Nature (London)* **442**, 282 (2006).
- ⁹M. Huang, O. Choi, Y. S. Ju, and H. T. Hahn, *Appl. Phys. Lett.* **89**, 023117 (2006).
- ¹⁰P. Sozzani, S. Bracco, A. Comotti, R. Simonutti, P. Valsesia, Y. Sakamoto, and O. Terasaki, *Nat. Mater.* **5**, 545 (2006).
- ¹¹M. N. Baibich, J. M. Broto, A. Fert, F. N. Vandau, F. Petroff, P. Eitanne, G. Creuzet, A. Friederich, and J. Chazelas, *Phys. Rev. Lett.* **61**, 2472 (1988).
- ¹²M. M. Miller, P. E. Sheehan, R. L. Edelstein, C. R. Tamanaha, L. Zhong, S. Bounnak, L. J. Whitman, and R. J. Colton, *J. Magn. Magn. Mater.* **225**, 138 (2001).
- ¹³A. Moser, K. Takano, D. T. Margulies, M. Albrecht, Y. Sonobe, Y. Ikeda, S. H. Sun, and E. E. Fullerton, *J. Phys. D* **35**, R157 (2002).
- ¹⁴C. Giebeler, D. J. Adelerhof, A. E. T. Kuiper, J. B. A. van Zon, D. Oelgeschlager, and G. Schulz, *Sens. Actuators, A* **91**, 16 (2001).
- ¹⁵R. C. Advincula, *J. Dispersion Sci. Technol.* **24**, 343 (2003).
- ¹⁶G. K. Jennings and E. L. Brantley, *Adv. Mater. (Weinheim, Ger.)* **16**, 1983 (2004).
- ¹⁷Z. Guo, S. Park, and H. T. Hahn, AICHE Annual Meeting, San Francisco, 2006 (unpublished).
- ¹⁸Standard XRD file: PDF Card No. 06-0696.
- ¹⁹Standard XRD file: PDF Card No. 39-1346.
- ²⁰B. D. Cullity, *Introduction to Magnetic Materials* (Addison-Wiley, New York, 1972), p. 617.
- ²¹D. Zhang, K. J. Klabunde, C. M. Sorensen, and G. C. Hadjipanayis, *Phys. Rev. B* **58**, 14167 (1998).
- ²²D. Kechrakos and K. N. Trohidou, *Phys. Rev. B* **58**, 12169 (1998).
- ²³V. Skumryev, S. Stoyanov, Y. Zhang, G. Hadjipanayis, D. Givord, and J. Nogues, *Nature (London)* **423**, 850 (2003).
- ²⁴P. Sheng, *Phys. Rev. Lett.* **31**, 44 (1973).
- ²⁵D. L. Graham, H. A. Ferreira, and P. P. Freitas, *Trends Biotechnol.* **22**, 455 (2004).
- ²⁶P. K. Ghosh and L. Philip, *J. Environ. Sci. Health, Part B* **40**, 425 (2005).
- ²⁷J. W. Lee, H. S. Kim, J. Y. Lee, and J. K. Kang, *Appl. Phys. Lett.* **88**, 143126 (2006).